

Supplementary Information

TRPML2 in distinct states reveals the activation and modulation principles of the TRPML family

Philip Schmiede^{1,‡}, Dawid Jaślan^{2,‡}, Michael Fine³, Nidish Ponath Sadanandan⁴, Alexandra Hatton¹, Nadia Elghobashi-Meinhardt⁵, Christian Grimm^{2,4,6*}, and Xiaochun Li^{1,7*}

¹Department of Molecular Genetics, University of Texas Southwestern Medical Center, Dallas, TX 75390, USA.

²Department of Pharmacology and Toxicology, Medical Faculty, Ludwig Maximilian University of Munich, Munich, Germany.

³Department of Neuroscience, Bowdoin College, Brunswick, ME 04011, USA.

⁴Immunology, Infection and Pandemic Research IIP, Fraunhofer Institute for Translational Medicine and Pharmacology ITMP, Munich/Frankfurt, Germany.

⁵School of Chemistry, University College Dublin, South Belfield Dublin 4, Ireland.

⁶Department of Pharmacology, University of Oxford, Mansfield Rd, Oxford OX1 3QT, United Kingdom

⁷Department of Biophysics, University of Texas Southwestern Medical Center, Dallas, TX 75390, USA.

[‡]These authors contributed equally.

*To whom correspondence may be addressed. Email: Christian.Grimm@med.uni-muenchen.de or xiaochun.li@utsouthwestern.edu

Supplementary Fig. 1 Sequence alignment of human TRPML1, TRPML2, and TRPML3, gel filtration curves, and molecular structures of TRPML substrates.

Supplementary Fig. 2 Ligand structures and densities.

Supplementary Fig. 3 Ion pore measurements and comparisons of the reported structures.

Supplementary Fig. 4 Cryo-EM workflow and analysis of apo TRPML2 and (-)ML-SI3-bound TRPML2.

Supplementary Fig. 5 Cryo-EM workflow and analysis of the (+)ML-SI3-bound TRPML2 states.

Supplementary Fig. 6 Cryo-EM workflow and analysis of ML2-SA1-bound TRPML2 and ML2-SA1/PI(3,5)P₂-bound TRPML2.

Supplementary Fig. 7 Structural comparison of TRPML2 with other TRP channels and homologues.

Supplementary Fig. 8 Expression, localization, and electrophysiological validation of TRPML2 and TRPML1^{VA/AG} with ML2-SA1.

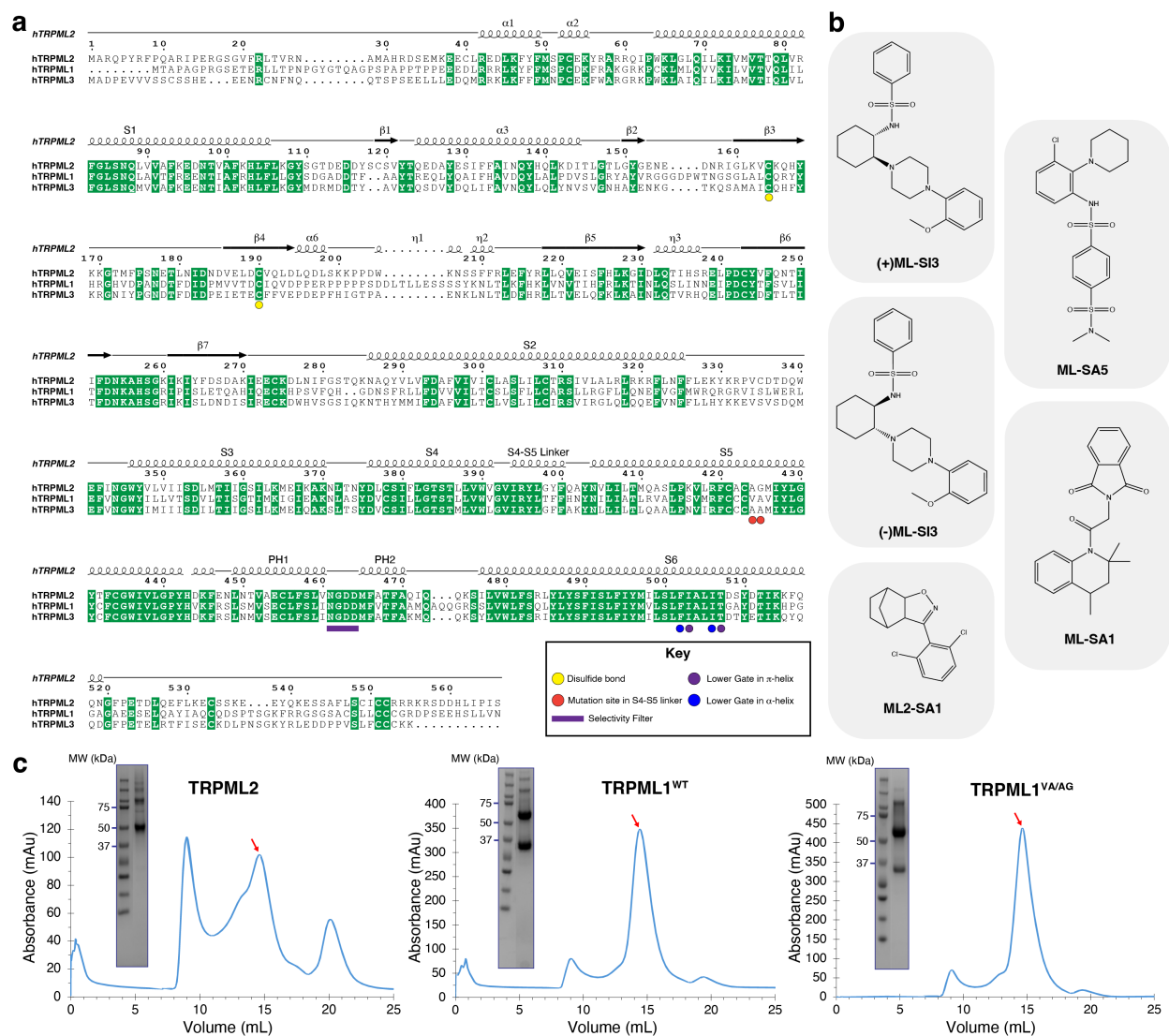
Supplementary Fig. 9 Cryo-EM workflow and analysis of ML2-SA1-bound TRPML1^{VA/AG}.

Supplementary Fig. 10 Cryo-EM workflow and analysis of (+)ML-SI3-bound TRPML1^{VA/AG} for both partially open and pre-open conformations and ML-SA5-bound TRPML1^{WT}.

Supplementary Fig. 11 Pore snapshots from molecular dynamics simulations

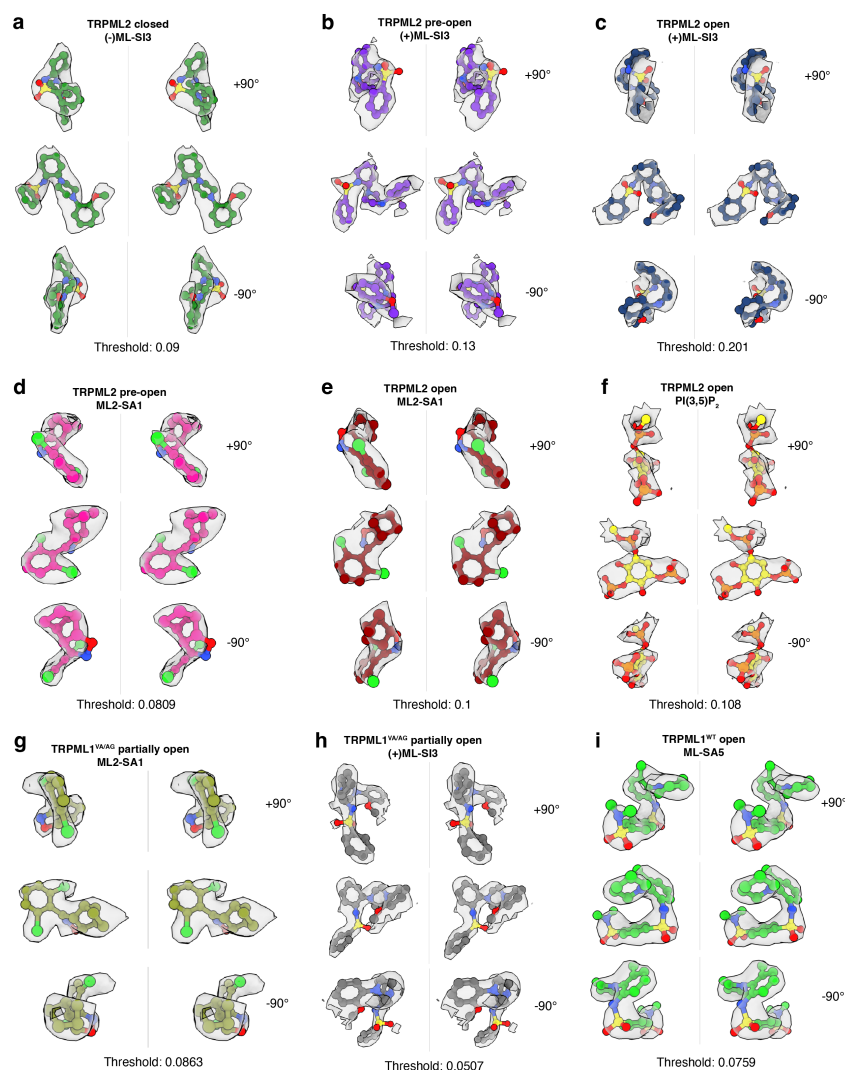
Supplementary Table 1: Cryo-EM data collection, refinement and validation statistics for TRPML2 structures

Supplementary Table 2: Cryo-EM data collection, refinement and validation statistics for TRPML1 structures



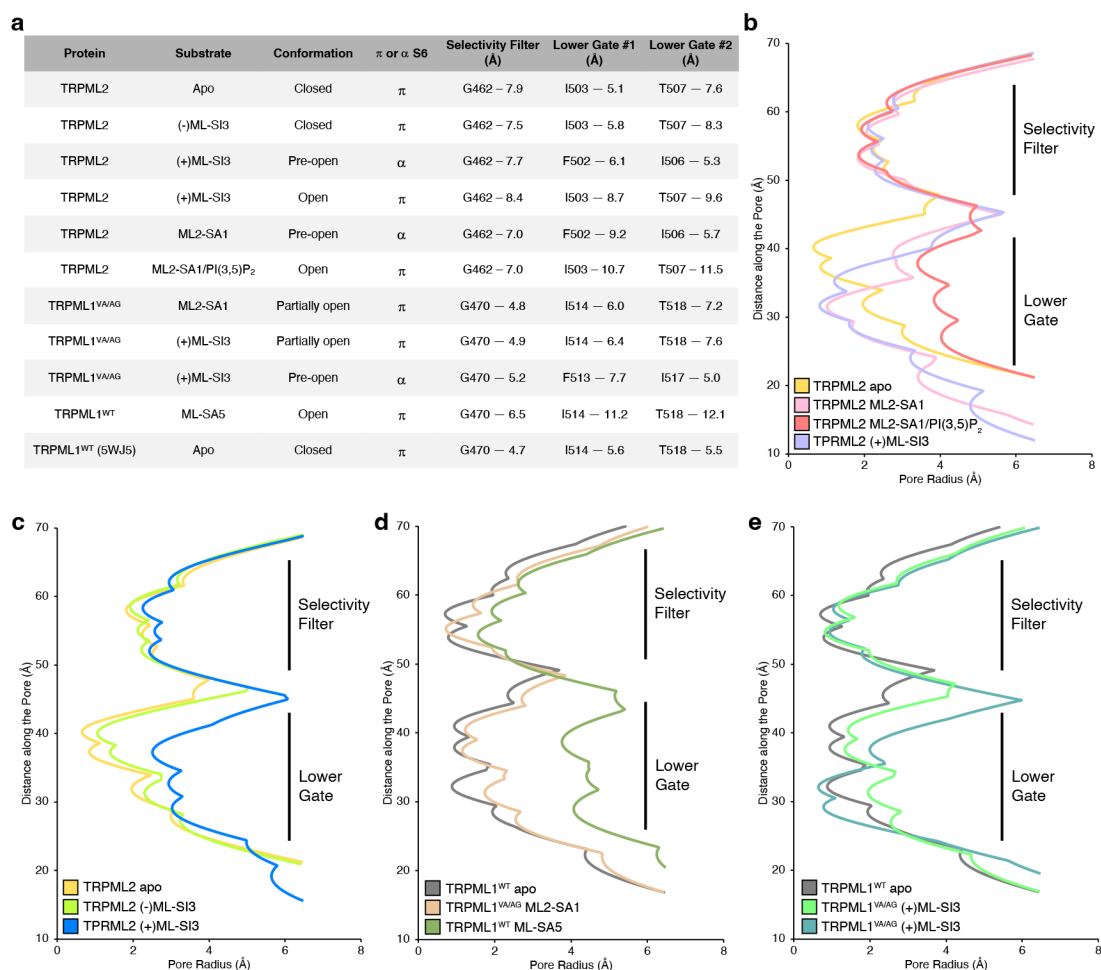
Supplementary Fig. 1 Sequence alignment of human TRPML1, TRPML2, and TRPML3, gel filtration curves, and molecular structures of TRPML substrates.

a. Sequence alignment shown with respect to TRPML2. Structural features of TRPML2 are shown along the top, with important residues from the paper indicated. **b.** Molecular structures of small molecule compounds that bind to TRPML channels in this work. **c.** The gel filtration chromatographs of the proteins purified for cryo-EM studies in this project. The red arrows indicate the peak fractions, with the accompanying SDS-PAGE gel. The degraded fragment of TRPML1 appears around 37 kDa on the SDS-PAGE.



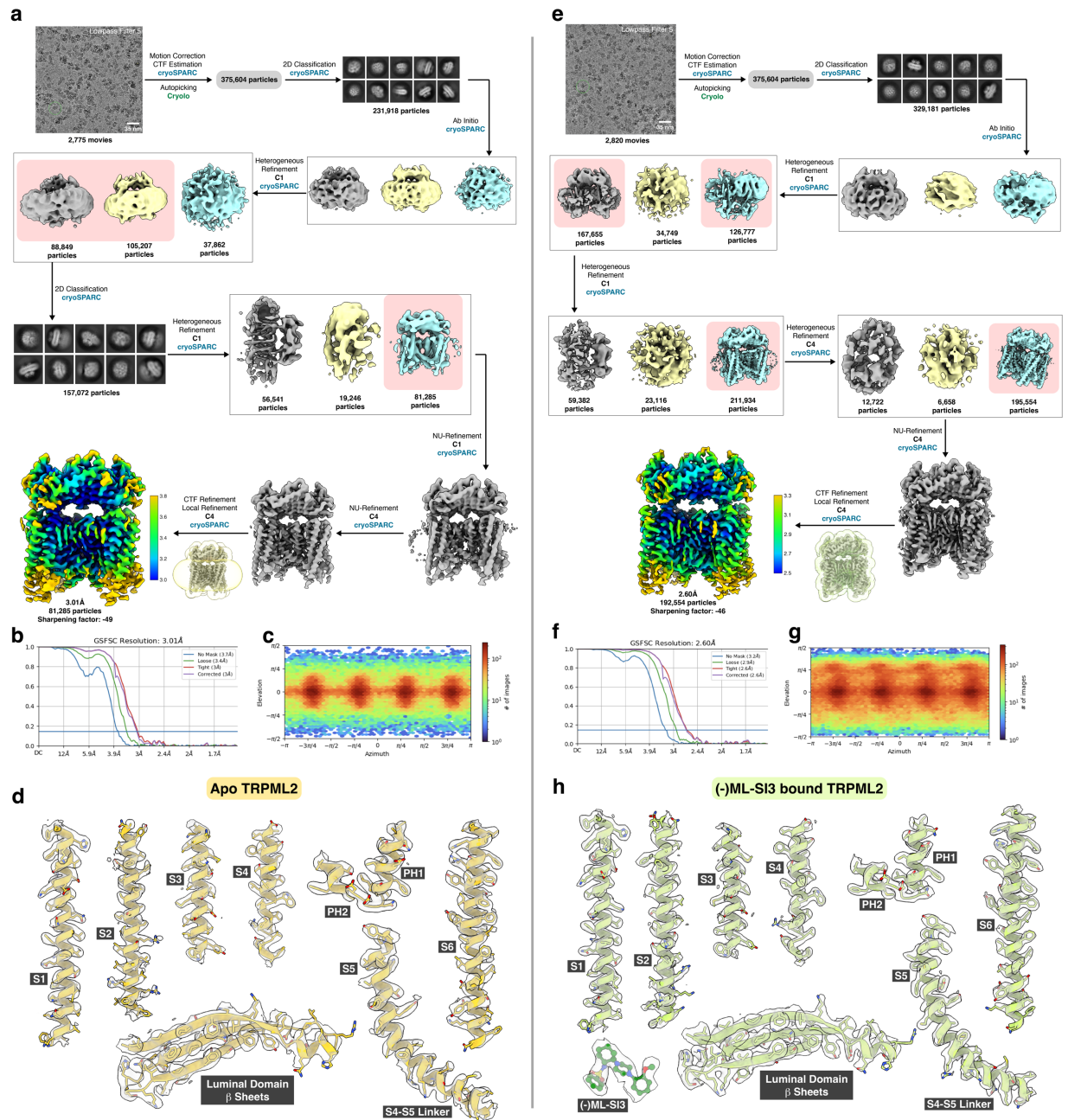
Supplementary Fig. 2 Ligand structures and densities.

a-f. Ligands from the structures in Fig. 1, colored as in Fig. 1: (-)ML-SI3 from the (-)ML-SI3 bound TRPML2 in a closed state (**a**), (+)ML-SI3 from the (+)ML-SI3 bound TRPML2 in a pre-open state (**b**), (+)ML-SI3 from the (+)ML-SI3 bound TRPML2 in an open state (**c**), ML2-SA1 from the ML2-SA1 bound TRPML2 in a pre-open state (**d**), ML2-SA1 from the ML2-SA1 bound TRPML2 in an open state (**e**), and PI(3,5)P₂ from the ML2-SA1/PI(3,5)P₂ bound TRPML2 in an open state (**f**). **g-i.** Ligands from the structures in Fig. 6, colored as in Fig. 6: ML2-SA1 from the ML2-SA1 bound TRPML1^{VA/AG} in a partially open state (**g**), (+)ML-SI3 from the (+)ML-SI3 bound TRPML1^{VA/AG} in a partially open state (**h**), and ML-SA5 from the ML-SA5 bound TRPML1^{WT} in an open state (**i**). All compounds are shown in three different orientations with the different thresholds for the density maps indicated below.



Supplementary Fig. 3 Ion pore measurements and comparisons of the reported structures.

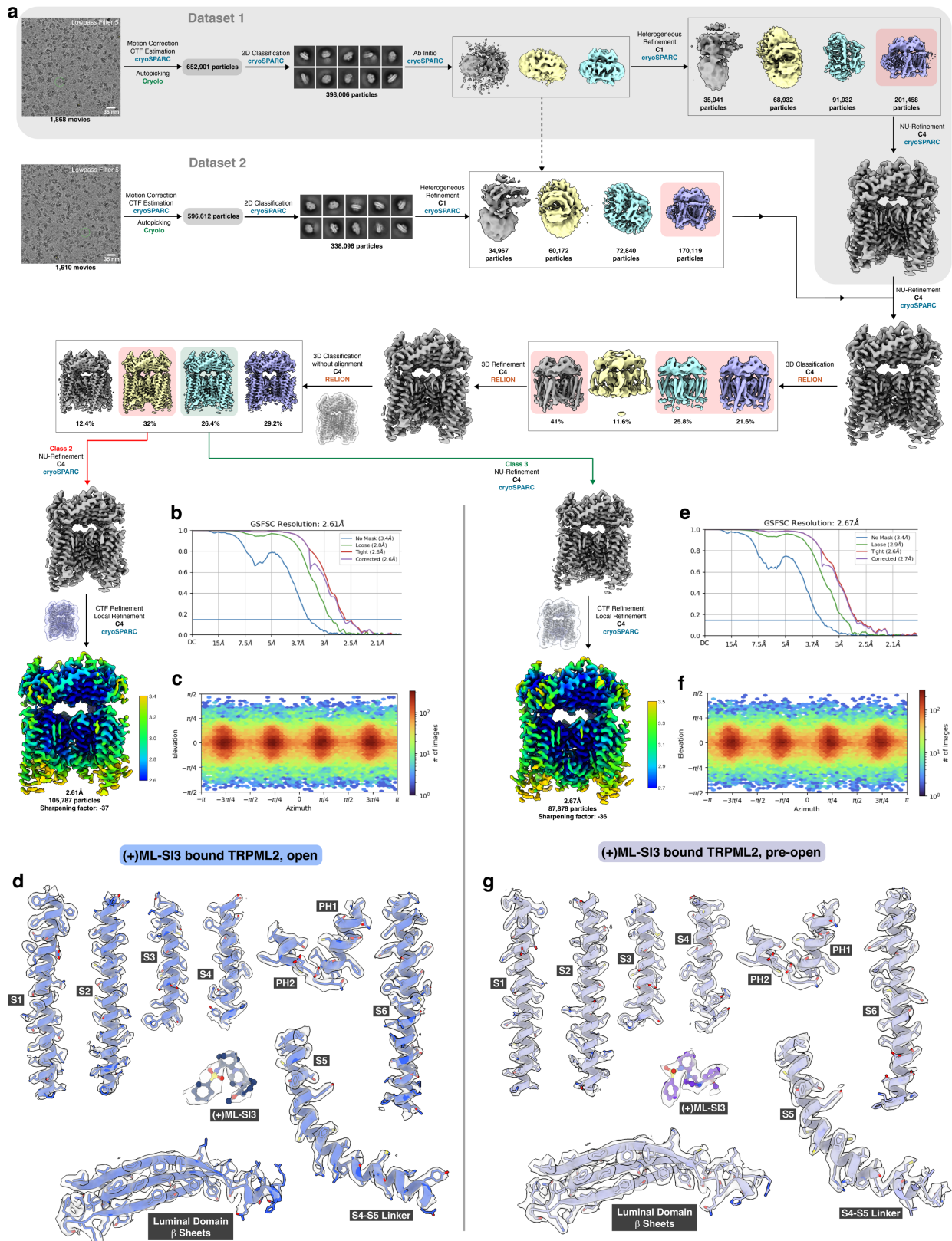
a. Summary of the distances between residues of the selective filter and lower gate in the reported structures. **b-c.** Comparison of the pore radius for the TRPML2 structures, as calculated by HOLE, colored as in Fig. 1. **d-e.** Comparison of pore radius for the TRPML1^{WT} and TRPML1^{VA/AG} structures, as calculated by HOLE, colored as in Fig. 6.



Supplementary Fig. 4 Cryo-EM workflow and analysis of apo TRPML2 and (-)-ML-SI3-bound TRPML2.

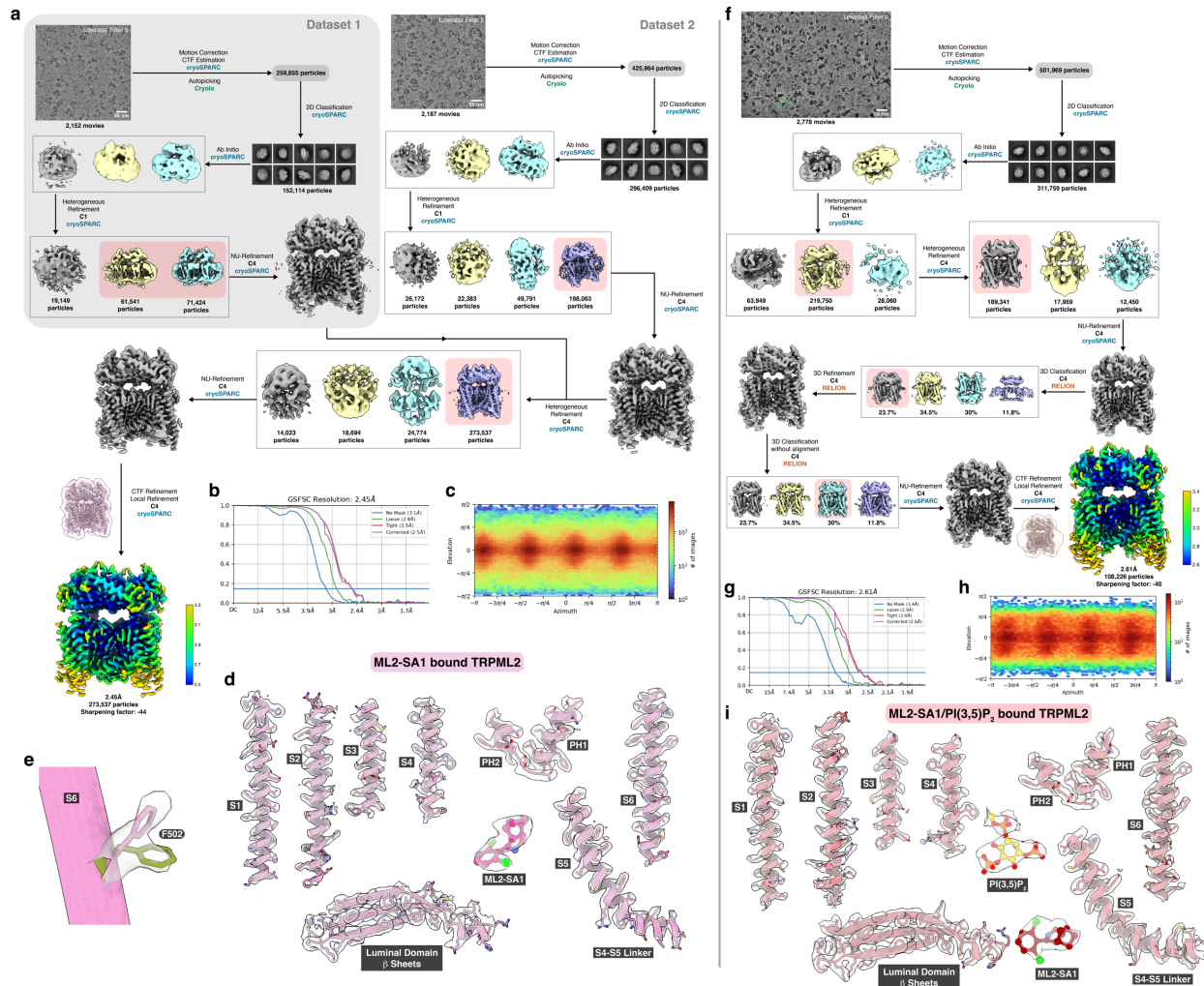
a. Summary of the image processing procedures of apo TRPML2. The final map is colored by local resolution estimation using cryoSPARC. The micrograph is a cropped representative image of the protein sample on the grid. **b.** Fourier shell correlation (FSC) curves of the final reconstruction from cryoSPARC. **c.** Representation of the angular distribution of the particles used in the final reconstruction from cryoSPARC. **d.** Major structural features of apo TRPML2 with the

structural model shown as cartoons and colored as in Fig. 1, and map density in gray. **e.** Summary of the image processing procedures of (-)ML-SI3-bound TRPML2. The final map is colored by local resolution estimation using cryoSPARC. The micrograph is a cropped representative image of the protein sample on the grid. **f.** Fourier shell correlation (FSC) curves of the final reconstruction from cryoSPARC. **g.** Representation of the angular distribution of the particles used in the final reconstruction from cryoSPARC. **h.** Major structural features of (-)ML-SI3-bound TRPML2 with the structural model shown as cartoons and colored as in Fig. 1, and map density in gray.



Supplementary Fig. 5 Cryo-EM workflow and analysis of the (+)ML-SI3-bound TRPML2 states.

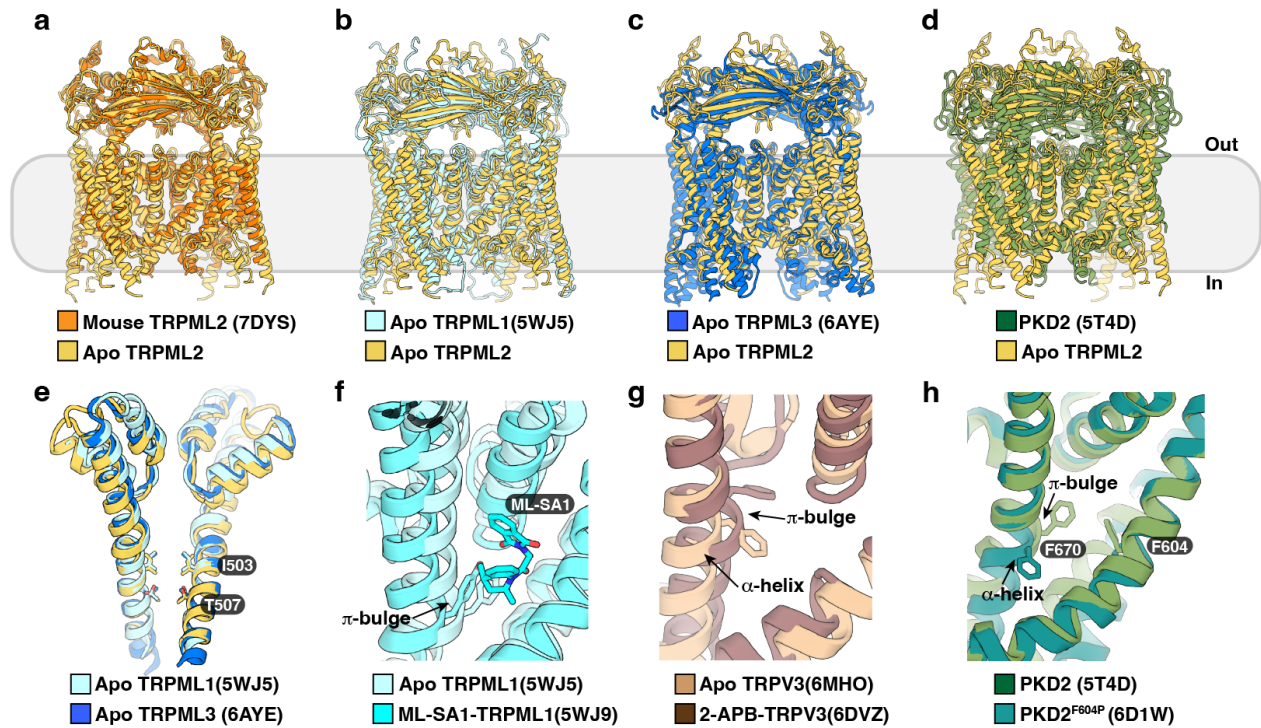
a. Summary of the image processing procedures of both (+)ML-SI3-bound TRPML2 states. Two datasets are indicated with Dataset 1 highlighted in gray. The final maps are colored by local resolution estimation using cryoSPARC. The micrographs are cropped representative images of the protein samples on the grid. **b.** Fourier shell correlation (FSC) curves of the final reconstruction of the open state from cryoSPARC. **c.** Representation of the angular distribution of the particles used in the final reconstruction of the open state from cryoSPARC. **d.** Major structural features of the open state of (+)ML-SI3-bound TRPML2 with the structural model shown as cartoons and colored as in Fig. 1, and map density in gray. **e.** Fourier shell correlation (FSC) curves of the final reconstruction of the pre-open state of (+)ML-SI3-bound TRPML2 from cryoSPARC. **f.** Representation of the angular distribution of the particles used in the final reconstruction of the pre-open state of (+)ML-SI3-bound TRPML2 from cryoSPARC. **g.** Major structural features of the pre-open state of (+)ML-SI3-bound TRPML2 with the structural model shown as cartoons and colored as in Fig. 1, and map density in gray.



Supplementary Fig. 6 Cryo-EM workflow and analysis of ML2-SA1-bound TRPML2 and ML2-SA1/PI(3,5)P₂-bound TRPML2.

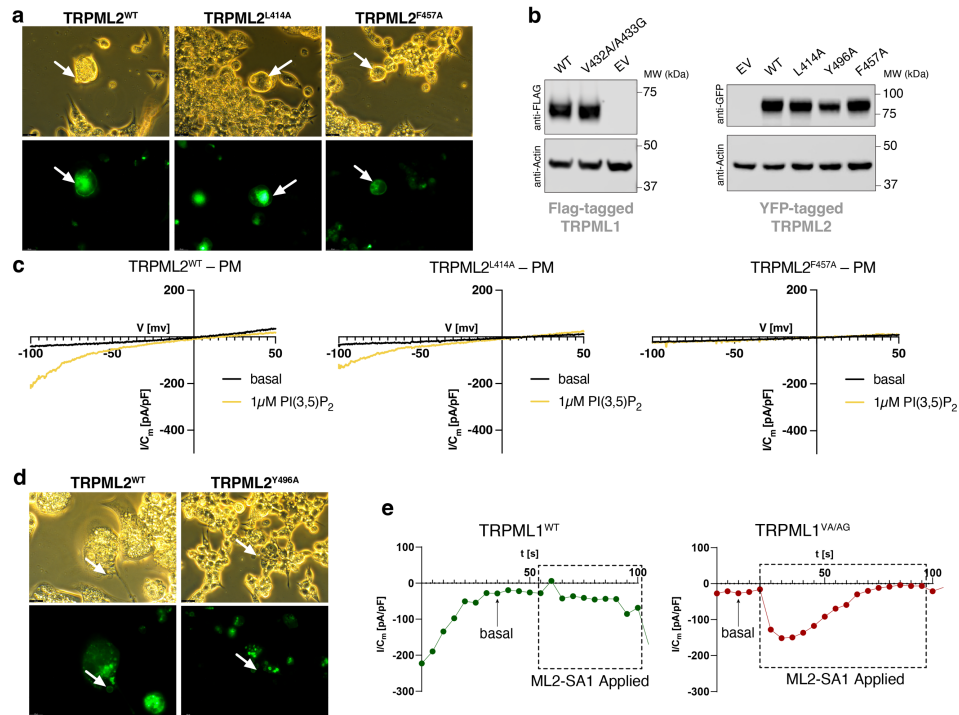
a. Summary of the image processing procedures of ML2-SA1-bound TRPML2. The final map is colored by local resolution estimation using cryoSPARC. The micrograph is a cropped representative image of the protein sample on the grid. **b.** Fourier shell correlation (FSC) curves of the final reconstruction from cryoSPARC. **c.** Representation of the angular distribution of the particles used in the final reconstruction from cryoSPARC. **d.** Major structural features of ML2-SA1-bound TRPML2 with the structural model shown as cartoons and colored as in Fig. 1, and map density in gray. **e.** Density of F502, showing the two different possible conformations of that residue with the S6 helix labeled. **f.** Summary of the image processing procedures of ML2-SA1/PI(3,5)P₂-bound TRPML2. The final map is colored by local resolution estimation using cryoSPARC. The micrograph is a cropped representative image of the protein sample on the grid.

g. Fourier shell correlation (FSC) curves of the final reconstruction from cryoSPARC. **h.** Representation of the angular distribution of the particles used in the final reconstruction from cryoSPARC. **i.** Major structural features of ML2-SA1/PI(3,5)P₂-bound TRPML2 with the structural model shown as cartoons and colored as in Fig. 1, and map density in gray.



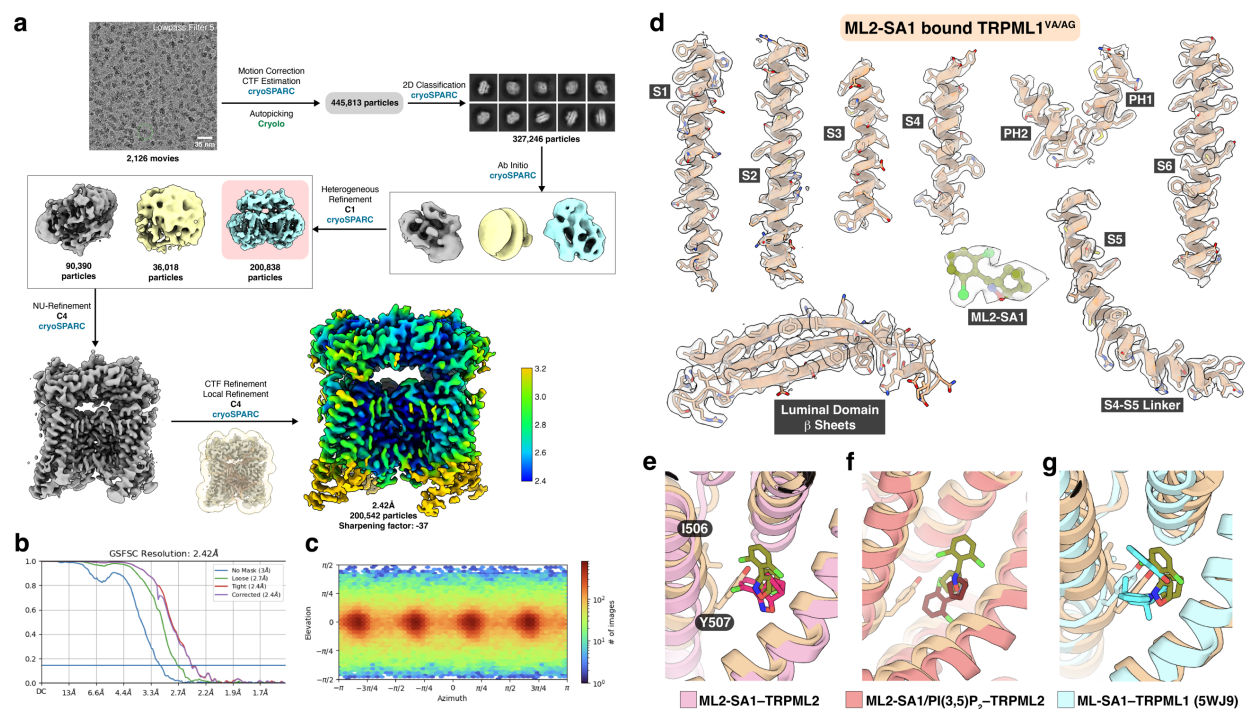
Supplementary Fig. 7 Structural comparison of TRPML2 with other TRP channels and homologues.

a. Structural comparison between apo human TRPML2 and mouse TRPML2. **b.** Structural comparison between apo human TRPML2 and apo TRPML1. **c.** Structural comparison between apo human TRPML2 and apo TRPML3. **d.** Structural comparison between apo human TRPML2 and apo PKD2. **e.** Comparison of pore regions among apo TRPML1, TRPML2, and TRPML3. **f.** Structural comparison between apo human TRPML1 and ML-SA1-bound TRPML1. **g.** Structural comparison between apo TRPV3 and 2-APB-bound TRPV3. **h.** Structural comparison between wild-type PKD2 and PKD2^{F604P}.



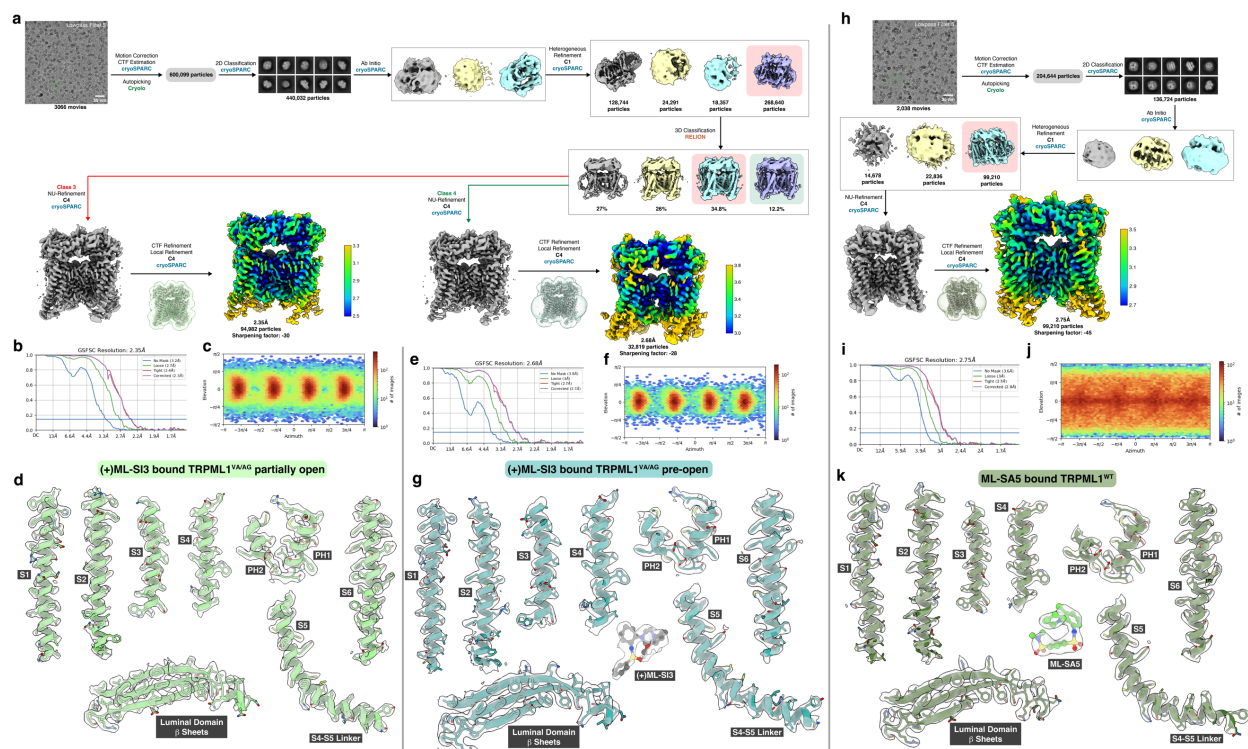
Supplementary Fig. 8 Expression, localization, and electrophysiological validation of TRPML2 and TRPML1^{VA/AG} with ML2-SA1.

a. Example of cellular localization of YFP-tagged TRPML2 constructs in transiently transfected HEK293 cells: WT (left), L414A (center), and F457A (right). **b.** Immunoblot analysis of FLAG-tagged TRPML1 constructs using with anti-Actin as a control (left). Immunoblot analysis of YFP-tagged TRPML2 constructs using with anti-Actin as a control (right). For both immunoblots, the constructs were expressed in transiently transfected HEK293 cells. Immunoblots were repeated at least 4 times with consistent results. **c.** Representative current density-voltage (I/C_m -V) relation of transiently expressed and plasma membrane localized human TRPML1-eYFP variants, WT (left), L414A mutant (center), and F457A mutant (right). Channels were activated by application of PI(3,5)P₂ (1 μ M, yellow). **d.** Example of enlarged and manually isolated endolysosomal vesicles transiently expressing TRPML2-YFP (WT and Y496A). **e.** Time course of current density recorded at -100 mV before and after the application of 10 μ M ML2-SA1 in endolysosomal compartments isolated from HEK293 cells transfected with TRPML1^{WT} or TRPML1^{VA/AG}.



Supplementary Fig. 9 Cryo-EM workflow and analysis of ML2-SA1-bound TRPML1^{VA/AG}.

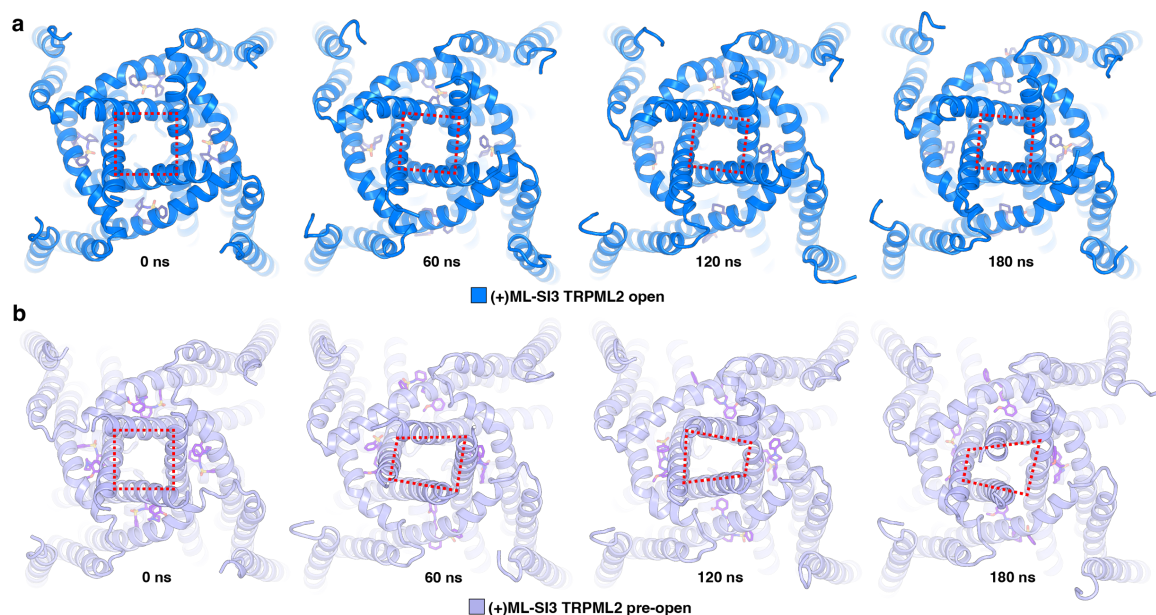
a. Summary of the image processing procedures of ML2-SA1-bound TRPML1^{VA/AG}. The final map is colored by local resolution estimation using cryoSPARC. The micrograph is a cropped representative image of the protein sample on the grid. **b.** Fourier shell correlation (FSC) curves of the final reconstruction from cryoSPARC. **c.** Representation of the angular distribution of the particles used in the final reconstruction from cryoSPARC. **d.** Major structural features of ML2-SA1-bound TRPML1^{VA/AG} with the structural model shown as cartoons and colored as in Fig. 5, and map density in gray. **e.** Superposition of ML2-SA1-bound TRPML2 (pink) with ML2-SA1-bound TRPML1^{VA/AG} (tan) with I506 and Y507 shown as sticks. **f.** Superposition of ML2-SA1/PI(3,5)P₂-bound TRPML2 (salmon) with ML2-SA1-bound TRPML1^{VA/AG} (tan) with Y507 shown as sticks. **g.** Superposition of ML-SA1-bound TRPML1 (5WJ9, cyan) with ML2-SA1-bound TRPML1^{VA/AG}.



Supplementary Fig. 10 Cryo-EM workflow and analysis of (+)ML-SI3-bound TRPML1^{VA/AG} for both partially open and pre-open conformations and ML-SA5-bound TRPML1^{WT}.

a. Summary of the image processing procedures of both states of (+)ML-SI3-bound TRPML1^{VA/AG}. The final maps are colored by local resolution estimation using cryoSPARC. The micrograph is a cropped representative image of the protein sample on the grid. **b.** Fourier shell correlation (FSC) curves of the final reconstruction of the partially open state of (+)ML-SI3-bound TRPML1^{VA/AG} from cryoSPARC. **c.** Representation of the angular distribution of the particles used in the final reconstruction of the partially open state of (+)ML-SI3-bound TRPML1^{VA/AG} from cryoSPARC. **d.** Major structural features of the partially open state of (+)ML-SI3-bound TRPML1^{VA/AG} with the structural model shown as cartoons and colored as in Fig. 5, and map density in gray. **e.** Fourier shell correlation (FSC) curves of the final reconstruction of the pre-open state of (+)ML-SI3-bound TRPML1^{VA/AG} from cryoSPARC. **f.** Representation of the angular distribution of the particles used in the final reconstruction of the pre-open state of (+)ML-SI3-bound TRPML1^{VA/AG} from cryoSPARC. **g.** Major structural features of the pre-open state of (+)ML-SI3-bound TRPML1^{VA/AG} with the structural model shown as cartoons and colored as in Fig. 5, and map density in gray. **h.** Summary of the image processing procedures of ML-SA5-bound TRPML1^{WT}. The final maps are colored by local resolution estimation using cryoSPARC.

The micrograph is a cropped representative image of the protein sample on the grid. **i.** Fourier shell correlation (FSC) curves of the final reconstruction of ML-SA5-bound TRPML1^{WT} from cryoSPARC. **j.** Representation of the angular distribution of the particles used in the final reconstruction of ML-SA5-bound TRPML1^{WT} from cryoSPARC. **k.** Major structural features of ML-SA5-bound TRPML1^{WT} with the structural model shown as cartoons and colored as in Fig. 6, and map density in gray.



Supplementary Fig. 11 Pore snapshots from molecular dynamics simulations

a. Snapshots of the transmembrane domain of (+)ML-SI3 bound TRPML2 in an open state (colored as in Fig. 1). The pore is viewed from the cytosolic side at the time points: 0 ns, 60 ns, 120 ns, and 180 ns. The red dashed-line square roughly indicates the size and shape of the pore. **b.** Snapshots of the transmembrane domain of (+)ML-SI3 bound TRPML2 in a pre-open state (colored as in Fig. 1). The pore is viewed from the cytosolic side at the time points: 0 ns, 60 ns, 120 ns, and 180 ns. The red dashed-line square roughly indicates the shape of the pore.

Supplementary Table 1: Cryo-EM data collection, refinement and validation statistics for TRPML2 structures

	Apo TRPML2 closed (EMDB-48139) (PDB-9EKW)	TRPML2 (-)ML-SI3 closed (EMDB-48140) (PDB-9EKX)	TRPML2 (+)ML-SI3 pre-open (EMDB-48141) (PDB-9EKY)	TRPML2 (+)ML-SI3 open (EMDB-48142) (PDB-9EKZ)	TRPML2 ML2-SA1 pre-open (EMDB-48143) (PDB-9EL0)	TRPML2 ML2-SA1/PI(3,5)P ₂ open (EMDB-48144) (PDB-9EL1)
Data collection and processing						
Normal Magnification	165kx	165kx	130kx		165kx	105kx
Voltage (kV)	300	300	300		300	300
Detector	Falcon 4i	Falcon 4i	Falcon 4i		Falcon 4i	Gatan K3
Electron exposure (e-/Å ²)	60	60	60		60	60
Defocus range (µm)	-0.8 to -1.8	-0.8 to -1.8	-0.8 to -1.8		-0.8 to -1.8	-0.8 to -1.8
Pixel size (Å)	0.738	0.738	0.936		0.738	0.826
Symmetry imposed	C4	C4	C4		C4	C4
Initial particle images (no.)	375,604	445,593	1,249,513		685,819	501,969
Final particle images (no.)	81,285	192,554	87,878	105,787	273,537	108,226
Initial movies (no.)	2,775	2,820	3,478		4,339	2,778
Map resolution (Å)	3.01	2.60	2.67	2.61	2.45	2.61
FSC threshold	0.143	0.143	0.143	0.143	0.143	0.143
Refinement						
Initial model used (PDB code)	AlphaFold	Apo TRPML2 (this paper)	Apo TRPML2 (this paper)	Apo TRPML2 (this paper)	Apo TRPML2 (this paper)	Apo TRPML2 (this paper)
Model resolution (Å)	3.4	2.8	2.8	2.7	2.8	2.8
FSC threshold	0.5	0.5	0.5	0.5	0.5	0.5
Map sharpening <i>B</i> factor (Å ²)	-49	-46	-36	-37	-44	-40
Model composition						
Non-hydrogen atoms	15,188	15,324	15,216	15,312	14,832	15,364
Protein residues	1,868	1,868	1,836	1,844	1,816	1,844
Ligands	0	4	4	4	4	8
<i>B</i> factors (Å ²)						
Protein	123.72	72.15	85.05	90.48	92.36	88.38
Ligand	—	53.52	81.79	89.69	88.95	119.38
R.m.s. deviations						
Bond lengths (Å)	0.006	0.005	0.007	0.007	0.008	0.006
Bond angles (°)	1.101	0.739	0.950	0.871	1.277	1.025
Validation						
MolProbity score	1.70	1.48	1.66	1.40	1.48	1.76
Clashscore	6.85	5.63	8.31	7.25	7.90	9.62
Poor rotamers (%)	0.48	0.96	0.72	0.95	0.80	0.48
Ramachandran plot						
Favored (%)	95.44	96.96	96.67	98.23	97.77	96.25
Allowed (%)	4.56	3.04	3.33	1.77	2.23	3.75
Disallowed (%)	0	0	0	0	0	0

Supplementary Table 2: Cryo-EM data collection, refinement and validation statistics for TRPML1 structures

	TRPML1 ^{VA/AG} ML2-SA1 partially open (EMDB-48135) (PDB-9EKS)	TRPML1 ^{VA/AG} (+)ML-SI3 partially open (EMDB-48136) (PDB-9EKT)	TRPML1 ^{VA/AG} (+)ML-SI3 pre- open (EMDB- 48137) (PDB-9EKU)	TRPML1 WT ML-SA5 open (EMDB-48138) (PDB-9EKV)
Data collection and processing				
Normal Magnification	165kx	165kx		165kx
Voltage (kV)	300	300		300
Detector	Falcon 4i	Falcon 4i		Falcon 4i
Electron exposure (e-/Å ²)	60	60		60
Defocus range (μm)	-0.8 to -1.8	-0.8 to -1.8		-0.8 to -1.8
Pixel size (Å)	0.738	0.738		0.738
Symmetry imposed	C4	C4		C4
Initial particle images (no.)	445,813	600,099		204,644
Final particle images (no.)	200,542	94,982	32,819	99,210
Initial movies (no.)	2,126	3,066		2,038
Map resolution (Å)	2.42	2.35	2.68	2.75
FSC threshold	0.143	0.143	0.143	0.143
Refinement				
Initial model used (PDB code)	Apo TRPML1 (5WJ5)	Apo TRPML1 (5WJ5)	Apo TRPML1 (5WJ5)	ML-SA1 TRPML1 (5WJ9)
Model resolution (Å)	2.5	2.7	3.0	3.0
FSC threshold	0.5	0.5	0.5	0.5
Map sharpening <i>B</i> factor (Å ²)	-37	-30	-28	-45
Model composition				
Non-hydrogen atoms	14,536	14,052	13,956	15,117
Protein residues	1,804	1,756	1,732	1,860
Ligands	4	0	4	4
<i>B</i> factors (Å ²)				
Protein	89.51	56.90	92.46	58.58
Ligand	87.56	—	30.00	30.00
R.m.s. deviations				
Bond lengths (Å)	0.004	0.003	0.005	0.004
Bond angles (°)	0.963	0.579	1.167	0.536
Validation				
MolProbity score	1.65	1.61	1.65	1.37
Clashscore	7.54	6.46	8.68	4.86
Poor rotamers (%)	0.25	0.64	0.52	0.73
Ramachandran plot				
Favored (%)	96.39	96.29	96.94	97.39
Allowed (%)	3.61	3.71	3.06	2.61
Disallowed (%)	0	0	0	0